Received: 21 June 2024 | Revised: 26 August 2024 | Accepted: 24 September 2024

DOI: 10.1002/zamm.202400609

ZAMM

SPECIAL ISSUE ARTICLE

A size-dependent model of strain gradient elastic laminated micro-beams with a weak adhesive layer

Michele Serpilli[1] | **Raffaella Rizzoni**[2] | **Reinaldo Rodríguez Ramos**[3,4] | **Frédéric Lebon**[5]

[1]Department of Civil and Building Engineering, and Architecture, Università Politecnica delle Marche, Ancona, Italy

[2]Department of Engineering, University of Ferrara, Ferrara, Italy

[3]Facultad de Matemática y Computación, Universidad de La Habana, Havana, Cuba

[4]PPG-MCCT, Universidade Federal Fluminense, Rio de Janeiro, Brazil

[5]LMA, Aix Marseille University, CNRS, Centrale Marseille, Marseille, France

Correspondence
Michele Serpilli, Department of Civil and Building Engineering, and Architecture, Università Politecnica delle Marche, Ancona, Italy.
Email: m.serpilli@univpm.it

A size-dependent model for a laminated micro-beam with a soft adhesive is developed in the framework of strain gradient elasticity theory. The layered beam is constituted by two Euler–Bernoulli strain gradient elastic isotropic beams, joined through a strain gradient spring-type contact law at the adhesive level. The governing bending and extensional equations and boundary conditions are obtained by using the variational principle. The differential system shows a coupling between the flexural and axial behaviors of the upper and lower beams, due to the presence of interface terms related to shear and peeling stresses. Two benchmark problems have been presented through their closed-form solutions, namely a simply-supported laminated beam subjected to a uniform distributed load and a mode 2-type loading configuration of a layered axially deformable beam. Size effects and non-local phenomena, due to high strain concentrations, are highlighted. Though simple in their features, the examples prove the efficiency of the proposed approach in designing micro-scale layered beams.

1 | INTRODUCTION

The use of adhesive layers for bonded joints in composite materials presents numerous advantages, such as the ability to connect dissimilar materials and enhance the mechanical properties of the assembled structure. This process increases the performance of the individual components, thereby meeting specific requirements for strength and comfort. As a result, adhesive bonding technology has been extensively adopted in the fabrication of layered devices. Modeling bonded structures, such as laminates or sandwich beams, plates and shells, requires accuracy and a precise prediction of their mechanical behavior: in literature, a variety of theories and solution methods, such as the Finite Element (FE) Method, have been developed to tackle these problems, see, for example, the works by Caliri et al. [1–3].

Smart structures incorporating piezoelectric actuators and sensors [4–6], flexible electronics [7], and micro-electromechanical systems (MEMS) [8, 9] are some examples involving the bonding technology. The structural elastic behavior of MEMS has shown important differences with respect to the classical elastic results [10, 11]. Moreover, the impact of micro-scale adhesives has proved to affect the overall structural performance of the composite assemble, as shown experimentally in different papers [12–14]. The microstructural effects at these small scales are mainly due to the non-local interactions of stress and strain within the system. This non-local phenomenon, which induces size-dependent behavior, significantly impacts the mechanical response of micro-scale structures.

Being scale-free, linear and nonlinear elasticity theory cannot capture size effect phenomena and highlight the influence of the microstructure. That is why higher-order theories have been developed throughout the years to overcome the limitations of classical continuum mechanics. Mindlin [15, 16] can be considered the pioneer of the so-called strain gradient elastic theories, which accounts for the strains and their gradient as kinematical descriptors. These models incorporate numerous material length constants to evaluate the structural response. Due to the complexity in their evaluation, these models have been simplified by Aifantis and Askes [17–22] and generalized by Polizzotto [23–27]. For a detailed review of gradient elasticity theories, the reader can refer to the paper [28]. Regarding micro- and nano-sized beams, several theoretical papers are devoted to the study of strain gradient elastic Euler–Bernoulli beam models, such as: the one-scale length parameter model derived by Lazopoulos and Lazopoulos [29] and Xu et al. [30] are based on the simplified strain gradient elasticity theory [17, 18]; the variational formulation of Euler–Bernoulli micro-beam model has been treated by Niiranen et al. [31], studying the well-posedness of the problem which guarantees optimal convergence for conforming Galerkin discretization methods. Some of these models have been extended to shear-deformable Timoshenko beams [32] or functionally graded materials [33]. The closed-form solution for the bending of a bi-layered beam subjected to an external moment was calculated by Li et al. [34]; Sidhardh and Ray [35] proposed the mathematical formulation of the equilibrium of sandwich microbeams, considering strain gradient effects; Guangyang et al. [36] and Long et al. [37] developed size-dependent laminated strain gradient beam model, partially covered by a thin layer and also modeling the adhesive contact.

An accurate theoretical modeling of the bonded joint is essential in engineering design. The adhesive layer is classically treated as a thin interphase. By decreasing its thickness to zero, the interphase reduces to a two-dimensional surface, called the imperfect interface, on which ad-hoc jump conditions of selected physical fields are considered, for example, displacements and stresses. The spring-type interface is an example of a simple contact law according to which the stress vector is continuous at the interface and connected to the jump of the displacements through a stiffness tensor. Employing the asymptotic analysis, it has been shown that the spring-type arises as the limit behavior of a very thin layer made of a soft elastic material [38–41]. These asymptotic imperfect interface models have been generalized in different multiphysics settings [42, 43], such as coupled thermoelasticity [44], piezoelectricity [45, 46], magneto-electro-thermo-elasticity [47] and poroelasticity [48], and also applied in the modeling of laminated elastic beams and plates, comprising an adhesive weak layer [49–52]. Nevertheless, the aforementioned models are unable to accurately describe the mechanical behavior of materials with size-dependent phenomena, which become predominant as the composite size scales down. To take into account the influence of the inner microstructure among the composite constituents, the elastic contact laws have been recently generalized in the framework of micropolar elasticity [53], flexoelectricity [54], and strain gradient elasticity [55].

The present paper aims to provide an original model of a strain gradient elastic laminated beam, comprising a soft adhesive, modeled by means of the imperfect soft interface conditions obtained in Serpilli et al. [55]. This work seeks to take a step forward compared with other contributions dealing with similar topics, which do not take into account imperfect contact conditions at the interface among each lamina [35, 36] or the strain gradient nature of the adherents [37]. The laminated beam is constituted by two Euler–Bernoulli strain gradient elastic isotropic beams (adherents), characterized by one scale length parameter, joined through a size-dependent spring-type contact law at the adhesive level. The models are obtained through classical variational tools. The governing equations for the bending and extensional equilibrium problems are derived with the associated boundary conditions. The differential system shows a coupling between the flexural and axial behaviors of the upper and lower beams, due to the presence of some terms related to the interface shear and peeling stresses. Finally, two simple analytical and numerical examples have been formulated, considering a simply-supported laminated beam subjected to a uniform distributed load and a mode 2-type loading configuration of a layered axially deformable beam. The results highlight a strong influence of the adhesive internal length parameter and strain gradient concentrations at the beam extremities.

The outline of the paper is the following. Section 2 presents a summary of the asymptotic model for strain gradient elastic soft interface. In Section 3, the size-dependent model for a laminated strain gradient beam is presented, with the governing equations of the problem. Section 4 is devoted to the analytical and numerical assessment of the above model with two benchmark problems: (i) bending of a simply supported strain gradient elastic laminated beam under distributed constant loading; (ii) a mode 2-type axial problem for a strain gradient elastic laminated beam. Although simple in their features, the analytical examples prove to be efficient in assessing the impact of the thin adhesive on the structural behavior of the overall system. Section 5 contains concluding remarks addressing these findings.

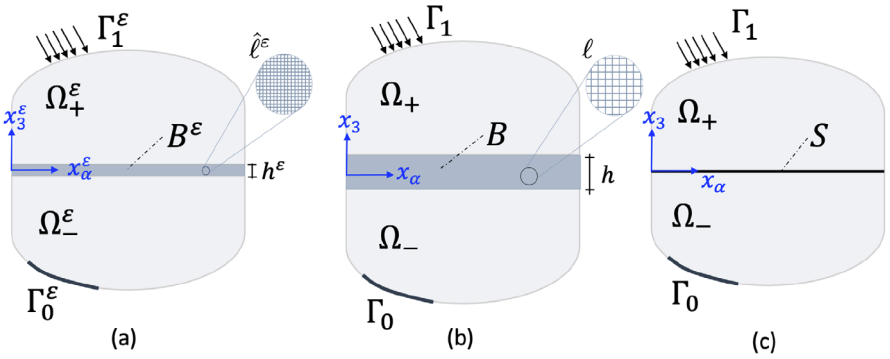

FIGURE 1 Initial (a), rescaled (b), and limit (c) configurations of the composite.

2 | AN OVERVIEW OF THE ASYMPTOTIC MODEL FOR SOFT STRAIN GRADIENT INTERFACES

In this Section, a summary of the results of the asymptotic analysis employed for the derivation of a soft strain gradient elastic interface model [55] is presented. The asymptotic methods provide an explicit expression of the contact laws in terms of the jumps and mean values of the stress and double stress vector evaluated at the interface. In what follows, Einstein's summation convention is used, Latin indices take values in the set $\{1, 2, 3\}$, while Greek indices are in the set $\{1, 2\}$.

Let us consider a small parameter $0 < \varepsilon < 1$. The composite assembly is composed by two media $\Omega_\pm^\varepsilon \subset \mathbb{R}^3$, called the adherents, bonded together by a thin plate-like layer $B^\varepsilon := S \times (-\frac{h^\varepsilon}{2}, \frac{h^\varepsilon}{2})$, called the adhesive, whose thickness depends linearly on ε, that is, $h^\varepsilon = \varepsilon h$, with cross-section $S \subset \mathbb{R}^2$. We note with $S_\pm^\varepsilon$ the interfaces between the adherents and the adhesives and $\Omega^\varepsilon := \Omega_+^\varepsilon \cup B^\varepsilon \cup \Omega_-^\varepsilon$ the reference configuration of the composite, see Figure 1a.

We assume that $\Omega_\pm^\varepsilon$ and B^ε are made of homogeneous strain gradient linear elastic materials, whose constitutive laws are defined as

$$\begin{cases} \sigma_{ij} = c_{ijhl} e_{hl}, \\ \tau_{ijk} = \ell^2 c_{ijhl} \eta_{hlk}, \end{cases} \tag{1}$$

where (σ_{ij}) and (τ_{ijk}) denote the Cauchy's stress tensor and the double-stress tensor, respectively, (c_{ijkl}) represents the elasticity tensor, ℓ is the internal length scale parameter, and $e_{ij} = \frac{1}{2}(u_{i,j} + u_{j,i})$, $\eta_{ijk} = e_{ij,k} = \frac{1}{2}(u_{i,jk} + u_{j,ik})$, with u_i the displacement field. Thus, we note with $\tilde{\sigma}_{ij} := \sigma_{ij} - \tau_{ijk,k} = c_{ijkl} e_{kl} - \ell^2 c_{ijhl} e_{hl,kk}$ the so-called total stress. In the case of an isotropic material, the elasticity tensor takes the form $c_{ijkl} = \lambda \delta_{ij} \delta_{kl} + \mu(\delta_{ik}\delta_{jl} + \delta_{il}\delta_{jk})$, with λ and μ the Lamé's constants.

The assembly is clamped on Γ_0^ε, with $u_i^\varepsilon = \partial_n^\varepsilon u_i^\varepsilon = 0$, and subjected to body forces f_i^ε, acting in $\Omega_\pm^\varepsilon$, and to surface forces g_i^ε, surface double forces q_i^ε, applied to the boundary $\Gamma_1^\varepsilon \subset \partial\Omega_\pm^\varepsilon$. The adhesive B^ε is supposed to be free of external loads. The equilibrium problem defined on the Ω^ε can be formulated in variational form as follows:

$$\begin{cases} \text{Find } \mathbf{u}^\varepsilon \in V(\Omega^\varepsilon), \quad \text{such that} \\ \bar{A}_-^\varepsilon(\mathbf{u}^\varepsilon, \mathbf{v}^\varepsilon) + \bar{A}_+^\varepsilon(\mathbf{u}^\varepsilon, \mathbf{v}^\varepsilon) + \hat{A}^\varepsilon(\mathbf{u}^\varepsilon, \mathbf{v}^\varepsilon) = L^\varepsilon(\mathbf{v}^\varepsilon), \quad \text{for all } \mathbf{v}^\varepsilon \in V(\Omega^\varepsilon), \end{cases} \tag{2}$$

where $V(\Omega^\varepsilon) := \{\bar{\mathbf{v}}^\varepsilon \in H^2(\Omega_\pm^\varepsilon, \mathbb{R}^3),\ \hat{\mathbf{v}}^\varepsilon \in H^2(B^\varepsilon, \mathbb{R}^3) :\ \bar{\mathbf{v}}^\varepsilon|_{S_\pm^\varepsilon} = \hat{\mathbf{v}}^\varepsilon|_{S_\pm^\varepsilon},\ \bar{\mathbf{v}}^\varepsilon_{,3}|_{S_\pm^\varepsilon} = \hat{\mathbf{v}}^\varepsilon_{,3}|_{S_\pm^\varepsilon},\ \bar{\mathbf{v}}^\varepsilon = \partial_n^\varepsilon \bar{\mathbf{v}}^\varepsilon = \mathbf{0} \text{ on } \Gamma_0^\varepsilon\}$, and $\bar{A}_\pm^\varepsilon(\cdot,\cdot)$ and $\hat{A}^\varepsilon(\cdot,\cdot)$ represent the bilinear forms associated with strain gradient elastic energy, defined on $\Omega_\pm^\varepsilon$ and B^ε, respectively, and $L^\varepsilon(\cdot)$ is the linear form related to the external source work:

$$\bar{A}_\pm^\varepsilon(\mathbf{u}^\varepsilon, \mathbf{v}^\varepsilon) := \int_{\Omega_\pm^\varepsilon} \left\{ \bar{c}_{ijhl}^\varepsilon e_{hl}^\varepsilon(\mathbf{u}^\varepsilon) e_{ij}^\varepsilon(\mathbf{v}^\varepsilon) + (\bar{\ell}^\varepsilon)^2 \bar{c}_{ijhl}^\varepsilon e_{hl,k}^\varepsilon(\mathbf{u}^\varepsilon) e_{ij,k}^\varepsilon(\mathbf{v}^\varepsilon) \right\} dx^\varepsilon,$$

$$\hat{A}^\varepsilon(\mathbf{u}^\varepsilon,\mathbf{v}^\varepsilon) := \int_{B^\varepsilon} \left\{ \hat{c}^\varepsilon_{ijhl} e^\varepsilon_{hl}(\mathbf{u}^\varepsilon) e^\varepsilon_{ij}(\mathbf{v}^\varepsilon) + (\hat{\ell}^\varepsilon)^2 \hat{c}^\varepsilon_{ijhl} e^\varepsilon_{hl,k}(\mathbf{u}^\varepsilon) e^\varepsilon_{ij,k}(\mathbf{v}^\varepsilon) \right\} dx^\varepsilon,$$

$$L^\varepsilon(\mathbf{v}^\varepsilon) := \int_{\Omega^\varepsilon_\pm} f^\varepsilon_i v^\varepsilon_i dx^\varepsilon + \int_{\Gamma^\varepsilon_1} \left\{ g^\varepsilon_i v^\varepsilon_i + q^\varepsilon_i \partial^\varepsilon_n v^\varepsilon_i \right\} d\Gamma^\varepsilon.$$

In the sequel, only if necessary, $\bar{\varphi}^\varepsilon$ and $\hat{\varphi}^\varepsilon$ will note the restrictions of functions φ^ε to $\Omega^\varepsilon_\pm$ and B^ε. In order to study the asymptotic behavior of the solution of problem (2), the following steps are classically carried out, see for example, [56]:

1. Change of variables: the variational problem is rewritten on a fixed domain Ω, independent of ε, through an appropriate transformation of coordinates, see Figure 1b.
2. Scaling assumptions on the data: the elastic coefficients and the characteristic length of $\Omega^\varepsilon_\pm$ are assumed to be independent of ε, namely $\bar{c}^\varepsilon_{ijkl} = \bar{c}_{ijkl}$, and $\bar{\ell}^\varepsilon = \bar{\ell}$. The elasticity tensor of B^ε and the internal scale length depend linearly on ε: $\hat{c}^\varepsilon_{ijkl} = \varepsilon \hat{c}_{ijkl}$, and $\hat{\ell}^\varepsilon = \varepsilon \ell$. The linear dependence of the elastic coefficients is typical of soft adhesives. The external loads are independent of ε, so that $f^\varepsilon_i(x^\varepsilon) = f_i(x)$, $x \in \Omega_\pm$, and $g^\varepsilon_i(x^\varepsilon) = g_i(x)$, $q^\varepsilon_i(x^\varepsilon) = q_i(x)$, $x \in \Gamma_1$.
3. The rescaled problem defined on the fixed domain Ω takes a polynomial structure with respect to ε. Thus, we can suppose an asymptotic expansion of the solution as a series of powers of ε: $\mathbf{u}^\varepsilon = \mathbf{u}^0 + \varepsilon \mathbf{u}^1 + \varepsilon^2 \mathbf{u}^2 + \cdots$.
4. By substituting the asymptotic development into the rescaled problem, we can finally characterize its leading term $\mathbf{u}^0$, and also higher-order terms, such as $\mathbf{u}^1$, and their associated limit equilibrium problems.

In the sequel, the results of Serpilli et al. [55] are presented considering only the order 0 interface conditions for a soft strain gradient elastic interface. The following equilibrium system on the adherents $\Omega_\pm$ is obtained:

$$\begin{cases} \bar{\tilde{\sigma}}^0_{ij,j} + f_i = 0 & \text{in } \Omega_\pm, \\ \bar{T}^0_i = g_i, \;\; \bar{R}^0_i = q_i & \text{on } \Gamma_1, \\ \bar{u}^0_i = 0, \;\; \partial_n \bar{u}^0_i = 0, & \text{on } \Gamma_0. \end{cases} \tag{3}$$

where $\bar{T}^0_i := \bar{\tilde{\sigma}}^0_{ij} n_j + \mathcal{D}^t_l(n_l) n_k n_j \bar{\tau}^0_{ijk} - \mathcal{D}^t_j(n_k \bar{\tau}^0_{ijk})$ and $\bar{R}^0_i := \bar{\tau}_{ijk} n_j n_k$ are, respectively, the traction vector and the higher-order traction vector on Γ_1, with $\mathcal{D}^t_i(\cdot) := (\delta_{ij} - n_i n_j)(\cdot)_{,j}$ the tangential derivative operator on the boundary with outer unit normal vector (n_i).

The above equations are matched together at the interface level by the transmission conditions for strain gradient elastic imperfect contact at order 0, in terms of the jumps and mean values of the stress vector $\bar{\mathbf{t}}^0 := (\bar{\tilde{\sigma}}^0_{i3} + \bar{\tau}^0_{i\alpha 3,\alpha})$ and double-stress vector $\bar{\mathbf{r}}^0 := (\bar{\tau}^0_{i33})$ evaluated at the interface:

$$\begin{cases} \left[\bar{\mathbf{t}}^0\right] = \mathbf{0}, \\ \langle \bar{\mathbf{t}}^0 \rangle = \frac{1}{h} f(l) \hat{\mathbf{K}}_{33} [\mathbf{u}^0], \\ \left[\bar{\mathbf{r}}^0\right] = \mathbf{0}, \\ \langle \bar{\mathbf{r}}^0 \rangle = \mathbf{0}, \end{cases} \tag{4}$$

with $f(l) := \frac{1}{1 - \frac{2}{l}\tanh\frac{l}{2}}$, $l := \frac{h}{\hat{\ell}}$, the internal length scale function, $\hat{\mathbf{K}}_{33} := (\hat{c}_{i3j3})$, and $[\varphi] := \varphi^+ - \varphi^-$ and $\langle \varphi \rangle := \frac{1}{2}(\varphi^+ + \varphi^-)$, $\varphi^\pm = \varphi|_{S_\pm}$, denote, respectively, the jump and mean values of the restrictions of φ at the interface $S_\pm$. It has been shown that by letting the internal length vanish $\hat{\ell} \to 0$, that is, $\lim_{l\to\infty} f(l) = 1$, the soft strain gradient elastic conditions converge towards the classical spring-type elastic interface law. Note that the characteristic length scale function $f(l)$ is responsible for the size dependency of the mechanical behavior of the composite.

2.1 | The variational formulation of the order 0 imperfect interface problem

Let us write the variational form of the equilibrium equations on each sub-domain Ω_+ and Ω_-, following the method proposed in ref. [42]. In the sequel, the '0' superscripts are omitted, for the sake of simplicity.

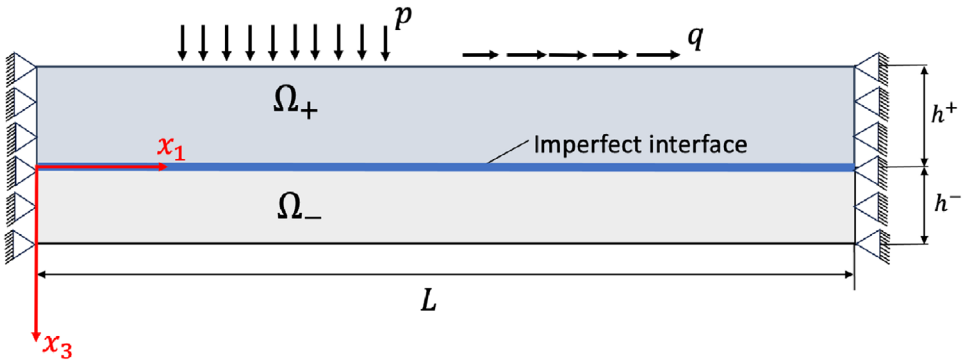

FIGURE 2 The geometry of the two-dimensional layered beam.

$$\int_{\Omega_\pm} \bar{\bar{\sigma}}_{ij} v_{i,j} dx - \int_S \left(\bar{t}_i^{\pm} v_i + \bar{r}_i^{\pm} v_{i,3}\right) dS = \int_{\Omega_\pm} f_i v_i dx + \int_{\Gamma_1} (g_i v_i + q_i \partial_n v_i) d\Gamma,$$

where $\bar{\bar{\sigma}}_{ij}$ represents the total stress in $\Omega_\pm$. The above expression is equivalent to:

$$\int_{\Omega_\pm} \bar{\bar{\sigma}}_{ij} v_{i,j} dx + \int_S \left([\bar{t}_i v_i] + [\bar{r}_i v_{i,3}]\right) dS = L(\mathbf{v}).$$

Using the property $[ab] = [a]\langle b\rangle + [b]\langle a\rangle$, one has

$$\int_{\Omega_\pm} \bar{\bar{\sigma}}_{ij} v_{i,j} dx + \int_S \left(\langle \bar{t}_i\rangle [v_i] + [\bar{t}_i]\langle v_i\rangle + [\bar{r}_i]\langle v_{i,3}\rangle + \langle \bar{r}_i\rangle [v_{i,3}]\right) dS = L(\mathbf{v}),$$

and, thus, by means of the expression of the interface conditions at order 0 (4), the variational formulation of the imperfect interface problem at order 0 can be rewritten as follows:

$$\begin{cases} \text{Find } \mathbf{u} \in \mathcal{V}(\Omega), \quad \text{such that} \\ \bar{A}_-(\mathbf{u},\mathbf{v}) + \bar{A}_+(\mathbf{u},\mathbf{v}) + \mathcal{A}(\mathbf{u},\mathbf{v}) = L(\mathbf{v}), \quad \text{for all } \mathbf{v} \in \mathcal{V}(\Omega), \end{cases} \tag{5}$$

with $\mathcal{V}(\Omega) := \{\mathbf{v}^\pm \in [H^2(\Omega_\pm)]^3,\ \mathbf{v} \in L^2(S),\ \mathbf{v}_{,3} \in L^2(S),\ \mathbf{v} = \mathbf{0},\ \partial_n \mathbf{v} = \mathbf{0} \text{ on } \Gamma_0\}$, and

$$\mathcal{A}(\mathbf{u},\mathbf{v}) := \frac{1}{h} \int_S f(l) \hat{\mathbf{K}}_{33}[\mathbf{u}] \cdot [\mathbf{v}] dS. \tag{6}$$

3 | THE SIZE-DEPENDENT MODEL FOR A LAMINATED COMPOSITE BEAM

For the present study, we consider a two-dimensional layered beam shown in Figure 2. The composite beam consists of a top beam Ω_+ bonded to the bottom one Ω_-, all along the adhesive joint. The total length of the beam is indicated by L, while h^+ and h^- represent, respectively, the thickness of the upper and lower beams. The x_1-axis is the axis of the beam, whereas the x_3-axis is the deflection axis. The elastica is defined on the deflection plane (x_1, x_3).

The mechanical assumptions adopted in the present study are summarized as follows:

1. The top and bottom beams are isotropic and linearly elastic strain gradient materials, with Young's moduli $E_\pm$, Poisson's ratio $\nu_\pm$ and internal length scale parameter ℓ_b.
2. The presence of the adhesive layer, of thickness h, is taken into account by means of the imperfect contact condition (4) for soft strain gradient interfaces, The adhesive is isotropic with Lamè's constants λ and μ, and internal length scale parameter ℓ_a.

3. The adherents are modeled by using the classical Euler–Bernoulli beam kinematics, so that

$$\begin{cases} u_1^{\pm}(x_1, x_3) := \bar{u}_{\pm}(x_1) - \left(x_3 \pm \frac{h^{\pm}}{2}\right) w'_{\pm}(x_1), \\ u_3^{\pm}(x_1, x_3) = w_{\pm}(x_1), \end{cases} \tag{7}$$

where $\bar{u}_{\pm}$ and $w_{\pm}$ represent the axial and transversal displacements of the upper and lower beams, respectively, and $(\cdot)' := \frac{d}{dx_1}(\cdot)$.

Considering the case of a two-dimensional laminated beam, with deformations in the deflection plane (x_1, x_3) and Euler–Bernoulli kinematics (7), the constitutive law reduces to [29]:

$$\begin{cases} \sigma_{11}^{\pm} = E^{\pm} e_{11}^{\pm} = E^{\pm}\left(\bar{u}'_{\pm} - \left(x_3 \pm \frac{h^{\pm}}{2}\right) w''_{\pm}\right), \\ \tau_{111}^{\pm} = \ell_b^2 E^{\pm} \eta_{111}^{\pm} = \ell_b^2 E^{\pm}\left(\bar{u}''_{\pm} - \left(x_3 \pm \frac{h^{\pm}}{2}\right) w'''_{\pm}\right), \\ \tau_{113}^{\pm} = \ell_b^2 E^{\pm} \eta_{113}^{\pm} = -\ell_b^2 E^{\pm} w''_{\pm}. \end{cases} \tag{8}$$

The interface variational problem (5) can be adapted to the present case and takes the following simplified form:

$$\begin{aligned} &\int_0^L \int_{-h^+}^0 \left(\sigma_{11}^+ e_{11}^+(\mathbf{v}) + \tau_{111}^+ \eta_{111}^+(\mathbf{v}) + \tau_{113}^+ \eta_{113}^+(\mathbf{v})\right) dx_1 dx_3 \\ &\quad + \int_0^L \int_0^{h^-} \left(\sigma_{11}^- e_{11}^-(\mathbf{v}) + \tau_{111}^- \eta_{111}^-(\mathbf{v}) + \tau_{113}^- \eta_{113}^-(\mathbf{v})\right) dx_1 dx_3 + \int_0^L \frac{f(l)}{h} (\mu [u_1][v_1] + (\lambda + 2\mu)[u_3][v_3]) dx_1 \\ &= \int_0^L \left(q^{\pm} \bar{v}_{\pm} + p^{\pm} \zeta_{\pm}\right) dx_1 + N_{\pm} \bar{v}_{\pm}\Big|_0^L + n_{\pm} \bar{v}'_{\pm}\Big|_0^L + V_{\pm} \zeta_{\pm}\Big|_0^L - M_{\pm} \zeta'_{\pm}\Big|_0^L + m_{\pm} \zeta''_{\pm}\Big|_0^L, \end{aligned} \tag{9}$$

where test functions $\mathbf{v} = (v_i)$ satisfy the Euler–Bernoulli kinematical assumptions, namely, $v_1^{\pm} = \bar{v}_{\pm}(x_1) - \left(x_3 \pm \frac{h^{\pm}}{2}\right) \zeta'_{\pm}(x_1)$ and $v_3^{\pm} = \zeta_{\pm}(x_1)$. We denote with $q^{\pm}$ and $p^{\pm}$ the axial and transversal distributed loads per unit length, respectively. Moreover, $N_{\pm}$, $n_{\pm}$, $V_{\pm}$, $M_{\pm}$ and $m_{\pm}$ represent the normal force, the normal double-force, the shear force, the bending moment and the bending double-moment evaluated at the extremities of the beam.

In Equation (9), $[u_1]$ and $[u_3]$ represent the jumps of the displacement at the interface between the upper and lower beams, for $x_3 = 0$. By using expression (7), we obtain that:

$$[u_1](x_1, 0) = [\bar{u}](x_1) - \langle\langle w' \rangle\rangle(x_1) \text{ and } [u_3](x_1, 0) = [w](x_1),$$

where $\langle\langle \varphi \rangle\rangle := \frac{1}{2}(h^+ \varphi^+ + h^- \varphi^-)$. Clearly, when $h^+ = h^- := h_b$, one has $\langle\langle \varphi \rangle\rangle := h_b \langle \varphi \rangle$. Similar expressions hold for the jumps of the test functions. By performing the integration along x_3, one has:

$$\begin{aligned} &\int_0^L \left(\Phi_{1,\pm} \zeta''_{\pm} + \Phi_{2,\pm} \zeta'''_{\pm}\right) dx_1 + \int_0^L \left(\Psi_{1,\pm} \bar{v}'_{\pm} + \Psi_{2,\pm} \bar{v}''_{\pm}\right) dx_1 + \int_0^L \left(\Lambda_1([\bar{v}] - \langle\langle \zeta' \rangle\rangle) + \Lambda_2[\zeta]\right) dx_1 \\ &= \int_0^L \left(q^{\pm} \bar{v}_{\pm} + p^{\pm} \zeta_{\pm}\right) dx_1 + N_{\pm} \bar{v}_{\pm}\Big|_0^L + n_{\pm} \bar{v}'_{\pm}\Big|_0^L + V_{\pm} \zeta_{\pm}\Big|_0^L - M_{\pm} \zeta'_{\pm}\Big|_0^L + m_{\pm} \zeta''_{\pm}\Big|_0^L, \end{aligned} \tag{10}$$

with

$$\begin{aligned} \Phi_{1,\pm} &:= E_{\pm}(I_{\pm} + \ell_b^2 A_{\pm}) w''_{\pm}, \quad & \Phi_{2,\pm} &:= \ell_b^2 E_{\pm} I_{\pm} w'''_{\pm} \\ \Psi_{1,\pm} &:= E_{\pm} A_{\pm} \bar{u}'_{\pm}, & \Psi_{2,\pm} &:= \ell_b^2 E_{\pm} A_{\pm} \bar{u}''_{\pm} \\ \Lambda_1 &:= \frac{f(l)}{h} \mu([\bar{u}] - \langle\langle w' \rangle\rangle), & \Lambda_2 &:= \frac{f(l)}{h} (\lambda + 2\mu)[w], \end{aligned} \tag{11}$$

where $I_{\pm} := \mp \int_{\mp h^{\pm}}^0 \left(x_3 \pm \frac{h^{\pm}}{2}\right)^2 dx_3 = \frac{(h^{\pm})^3}{12}$, and $A_{\pm} := \mp \int_{\mp h^{\pm}}^0 dx_3 = h^{\pm}$, represent the moments of inertia and cross-sectional areas of the adherents, respectively. Functions Λ_1 and Λ_2 are mechanically interpreted as the shear t_{13} and

peeling stresses t_{33} at the interface level. An integration by parts along the x_1-coordinate allows us to obtain the differential form of the equilibrium problem for a layered beam with imperfect contact and the associated boundary conditions, as follows:

$$\begin{cases} \textbf{Bending governing equations:} & \\ \Phi''_{1,\pm} - \Phi'''_{2,\pm} + \Lambda'_1 \frac{h^\pm}{2} \pm \Lambda_2 = p^\pm & x_1 \in (0,L), \\ \Phi''_{2,\pm} - \Phi'_{1,\pm} - \Lambda_1 \frac{h^\pm}{2} = V_\pm \text{ or } w = 0 & x_1 = 0, L, \\ \Phi'_{2,\pm} - \Phi_{1,\pm} = M_\pm \text{ or } w' = 0 & x_1 = 0, L, \\ \Phi_{2,\pm} = m \pm \text{ or } w'' = 0 & x_1 = 0, L, \\ \textbf{Extensional governing equations:} & \\ \Psi''_{2,\pm} - \Psi'_{1,\pm} \pm \Lambda_1 = q^\pm & x_1 \in (0,L), \\ \Psi_{1,\pm} - \Psi'_{2,\pm} = N_\pm \text{ or } \bar{u} = 0 & x_1 = 0, L, \\ \Psi_{2,\pm} = n_\pm \text{ or } \bar{u}' = 0 & x_1 = 0, L. \end{cases} \tag{12}$$

By substituting Equations (11) into (12), we get the explicit expression:

$$\begin{cases} \textbf{Bending governing equations:} & \\ E_\pm(I_\pm + \ell_b^2 A_\pm) w_\pm^{(4)} - \ell_b^2 E_\pm I_\pm w_\pm^{(6)} + \frac{h^\pm}{2}\frac{f(l)}{h}\mu([\bar{u}'] - \langle\langle w''\rangle\rangle) \pm \frac{f(l)}{h}(\lambda+2\mu)[w] = p^\pm & x_1 \in (0,L), \\ \ell_b^2 E_\pm I_\pm w_\pm^{(5)} - E_\pm(I_\pm + \ell_b^2 A_\pm) w'''_\pm - \frac{h^\pm}{2}\frac{f(l)}{h}\mu([\bar{u}] - \langle\langle w'\rangle\rangle) = V_\pm \text{ or } w = 0 & x_1 = 0, L, \\ \ell_b^2 E_\pm I_\pm w_\pm^{(4)} - E_\pm(I_\pm + \ell_b^2 A_\pm) w''_\pm = M_\pm \text{ or } w' = 0 & x_1 = 0, L, \\ \ell_b^2 E_\pm I_\pm w'''_\pm = m_\pm \text{ or } w'' = 0 & x_1 = 0, L, \\ \textbf{Extensional governing equations:} & \\ E_\pm A_\pm(\ell_b^2 \bar{u}_\pm^{(4)} - \bar{u}''_\pm) \pm \frac{f(l)}{h}\mu([\bar{u}] - \langle\langle w'\rangle\rangle) = q^\pm & x_1 \in (0,L), \\ E_\pm A_\pm(\bar{u}'_\pm - \ell_b^2 \bar{u}'''_\pm) = N_\pm \text{ or } \bar{u} = 0 & x_1 = 0, L, \\ \ell_b^2 E_\pm A_\pm \bar{u}''_\pm = n_\pm \text{ or } \bar{u}' = 0 & x_1 = 0, L, \end{cases} \tag{13}$$

where $(\cdot)^{(k)} := \frac{d^k}{dx_1^k}(\cdot)$ denotes the derivatives of order $k > 3$.

It is interesting to notice that the above differential system is fully coupled: the terms Λ_1 and Λ_2, associated with the imperfect contact model and containing the interface jumps $[\bar{u}]$, $[w]$ and mean values $\langle\langle w'\rangle\rangle$ of the axial and transversal displacements, induce the coupling not only of the upper and lower beams equations, but also of the extensional and bending behaviors. This observation is in full agreement with classical lamination theory and its extensions, such as zig–zag or piece-wise linear theories, according to which it is possible to prove that non-symmetric laminates show coupling effects between membrane forces and bending/torsion moments. The main difference with classical approaches consists in the use of the strain gradient elastic imperfect interface law (4), instead of continuity conditions for stresses and displacements among each lamina. The system can be likely decoupled by assuming, for instance, infinite axial stiffness or a particular choice of the adhesive elastic moduli. In the following sections, some simple numerical examples are proposed by decoupling the axial and bending mechanical behaviors. The presented model is a strain gradient generalization of the asymptotic models obtained in Serpilli and Lenci [50] by applying asymptotic techniques for three-layer elastic plates with an intermediate weak layer.

4 | TWO BENCHMARK PROBLEMS

In the sequel, two benchmark problems have been tackled in order to assess the above model from an analytical and numerical point of view. The first one is related to the bending equilibrium problem of a layered strain gradient elastic

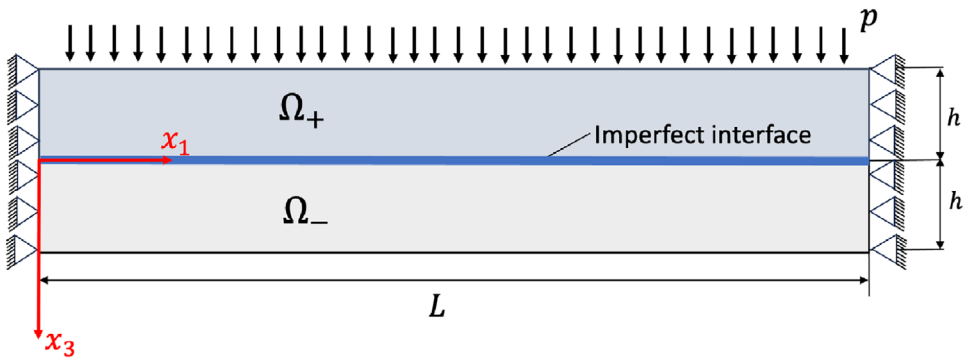

FIGURE 3 The simply supported strain gradient elastic laminated beam under distributed uniform load.

beam with soft strain gradient elastic adhesive subject to a transversal uniform load. The second one is associated with the problem of a mode 2-type axial load configuration. For the sake of simplicity and without loss of generality, the bending and axial problems are assumed to be decoupled in order to have simple closed-form solutions.

4.1 | Bending of a simply supported strain gradient elastic laminated beam under distributed constant loading

Let us consider a two-layer beam, whose bonded joint is made of an adhesive, modeled through the imperfect contact conditions expressed in (4) and whose governing equation is (13). Figure 3 illustrates the geometry of the beam. We assume that the top and bottom beams have the same thickness $h^+ = h^- := h_b$ ($I_+ = I_- := I$ and $A_+ = A_- := A$), material $E_+ = E_- := E$ and infinite axial stiffness so that the bending and extensional problems can be decoupled. The distributed uniform transversal load is applied on Ω_+. Moreover, both beams are supposed to be simply supported on the extremities at $x_1 = 0, L$. Thus, Equations (13) can be rewritten as follows:

$$\begin{cases} E(I+\ell_b^2 A)w_+^{(4)} - \ell_b^2 EIw_+^{(6)} - \frac{h_b^2}{2}\frac{f(l)}{h}\mu\langle w''\rangle + \frac{f(l)}{h}(\lambda+2\mu)[w] = p & x_1 \in (0,L), \\ E(I+\ell_b^2 A)w_-^{(4)} - \ell_b^2 EIw_-^{(6)} - \frac{h_b^2}{2}\frac{f(l)}{h}\mu\langle w''\rangle - \frac{f(l)}{h}(\lambda+2\mu)[w] = 0 & x_1 \in (0,L), \\ w_\pm = 0 & x_1 = 0, L, \\ w_\pm'' = 0 & x_1 = 0, L, \\ \ell_b^2 EIw_\pm^{(4)} - E_(I+\ell_b^2 A)w_\pm'' = 0 & x_1 = 0, L. \end{cases} \tag{14}$$

The above linear system can be easily decoupled on $\Omega_\pm$ by solving the problems involving the jump $[w]$ and mean value $\langle w\rangle$. By summing up and subtracting Equation (14), we get:

$$\begin{cases} \textbf{Jump equation:} & \\ E(I+\ell_b^2 A)[w^{(4)}] - \ell_b^2 EI[w^{(6)}] + \frac{2f(l)}{h}(\lambda+2\mu)[w] = p & x_1 \in (0,L), \\ [w] = 0 & x_1 = 0, L, \\ [w''] = 0 & x_1 = 0, L, \\ \ell_b^2 EI[w^{(4)}] - E(I+\ell_b^2 A)[w''] = 0 & x_1 = 0, L, \\ \textbf{Mean value equation:} & \\ E(I+\ell_b^2 A)\langle w^{(4)}\rangle - \ell_b^2 EI\langle w^{(6)}\rangle - \frac{h_b^2 f(l)}{2h}\mu\langle w''\rangle = \frac{p}{2} & x_1 \in (0,L), \\ \langle w\rangle = 0 & x_1 = 0, L, \\ \langle w''\rangle = 0 & x_1 = 0, L, \\ \ell_b^2 EI\langle w^{(4)}\rangle - E(I+\ell_b^2 A)\langle w''\rangle = 0 & x_1 = 0, L. \end{cases} \tag{15}$$

TABLE 1 Constitutive material properties for aluminum and PET [6, 37].

Material moduli	Al ($\Omega_{\pm}$)	PET (B)
E, GPa	70	3
ν, -	0.3	0

Abbreviations: Al, Aluminium; PET, polyethylene terephthalate.

TABLE 2 Adhesive thickness and internal lengths size ratios.

ℓ_a, mm	h/ℓ_a	ℓ_b/ℓ_a
1	1	0.1
0.1	10	1
0.01	100	10
0.001	1000	100
0	∞	∞

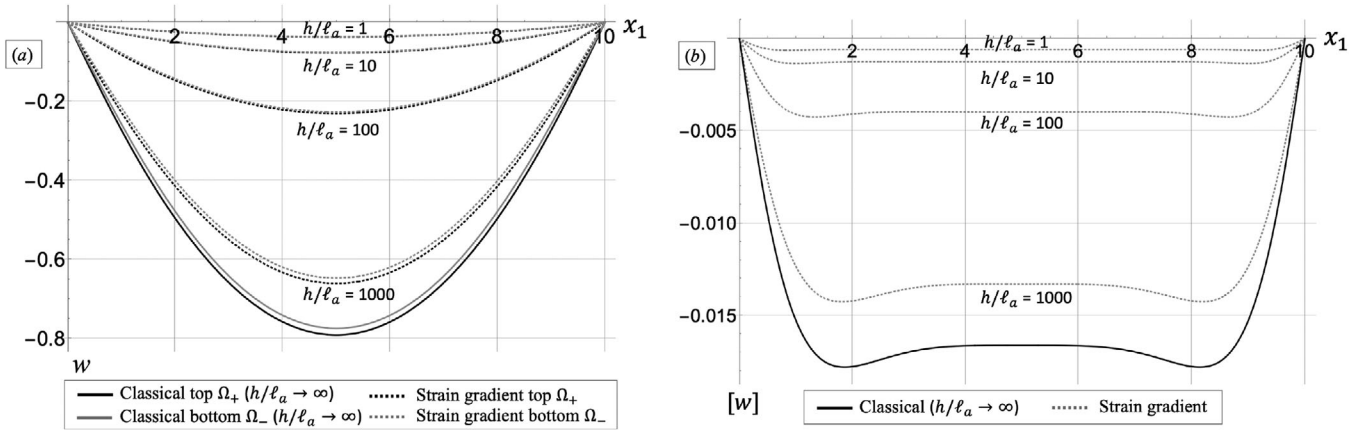

FIGURE 4 Transversal displacement w (a) and interfacial displacement jump $[w]$ (b) versus x_1.

Once the above system is solved, functions w_+ and w_- can be recovered as customary:

$$w_+(x_1) = \langle w\rangle(x_1) + \frac{1}{2}[w](x_1) \quad \text{and} \quad w_-(x_1) = \langle w\rangle(x_1) - \frac{1}{2}[w](x_1).$$

The jump and mean value equations admit the closed-form solutions:

$$[w](x_1) = c_1\cosh(\eta_1 x_1) + c_2\sinh(\eta_1 x_1) + \cosh(\gamma_1 x_1)(c_3\cos(\gamma_2 x_1) + c_4\sin(\gamma_2 x_1)) + \sinh(\gamma_1 x_1)(c_5\cos(\gamma_2 x_1) + c_6\sin(\gamma_2 x_1)) - \frac{P}{\alpha_3},$$

$$\langle w\rangle(x_1) = d_1\cosh(\delta_1 x_1) + d_2\sinh(\delta_1 x_1) + d_3\cosh(\delta_2 x_1) + d_4\sinh(\delta_2 x_1) + d_5 + d_6 x_1 + \frac{P}{4\alpha_4}x_1^2,$$

where $P := \frac{p}{l_b^2 EI}$, c_K and d_K, for $K = 1, \dots, 6$, are the integration constants to be found imposing the boundary conditions. Parameters η_α, γ_α, δ_α, for $\alpha = 1, 2$, α_3 and α_4 are defined in the Appendix.

Going to the numerical results, the adherents $\Omega_{\pm}$ are constituted by aluminum (Al), while the adhesive B is made of PET (polyethylene terephthalate), whose material properties are shown in Table 1. The adherents length is $L = 10$ mm, with thickness $h_b = 1$ mm and fixed internal length scale parameter $l_b = 0.1$ mm, and the adhesive thickness $h = 0.1$ mm. The distributed load is $p = 1$ kN/mm. The internal length of the adhesive ℓ_a takes different values, according to the size ratios presented in Table 2. In this way, we can monitor simultaneously the response of the laminated structure as the adhesive scale down (change of h/ℓ_a) and as the internal microstructure varies (change of ℓ_b/ℓ_a). Figure 4 shows the

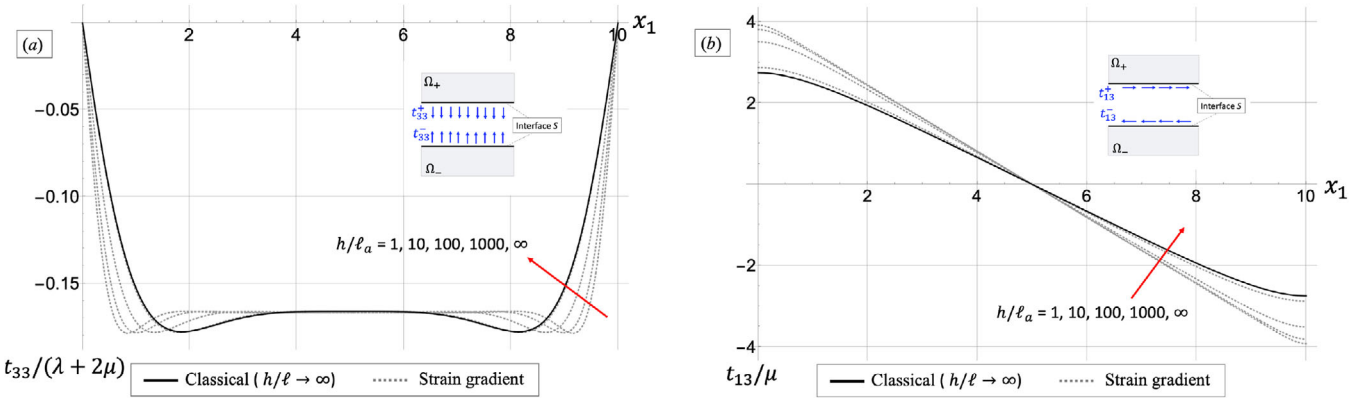

FIGURE 5 Normalized interfacial normal (a) and shear stresses (b) versus x_1.

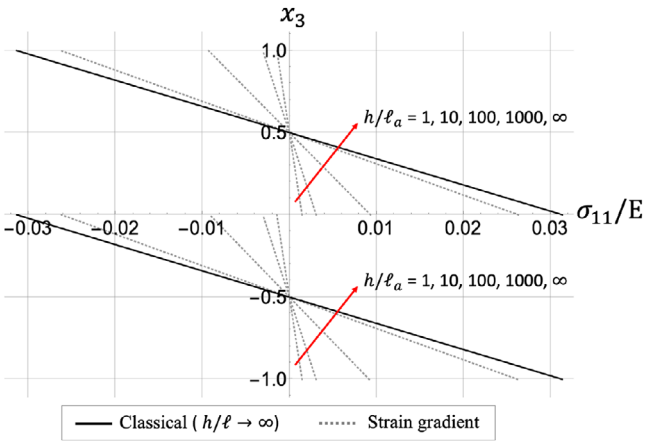

FIGURE 6 Variation of the normalized axial stress σ_{11} across the thickness of the laminated beam, for $x_1 = L/2$.

comparison between the classical elastic solution (black and gray continuous lines) and the strain gradient elastic solution (black and gray dotted lines) for different values of the size ratio h/ℓ_a in terms of the transversal displacement for the top and bottom beams, and interfacial jump. The plots highlight the influence of the adhesive characteristic length of the microstructure compared with the classical elastic solution, for which $h/\ell_a \to \infty$, that is, $\ell_a = 0$. As expected, the strain gradient solution approaches the elastic one, especially for high values of h/ℓ_a. This result is coherent with other size-dependent models for layered beams [37]. The internal length parameter influences the trend of the general solution and its effect becomes more prominent when $h/\ell_a = 1$. Indeed, when the characteristic length is of the same order of magnitude as the adhesive thickness, a stiffening phenomenon is highlighted, due to the high strain gradients. The strain gradient laminated beam appears to be more rigid with respect to the elastic one (Figure 4a), with a drastic decrease of the transversal displacements of both the upper and lower layers. Moreover, the size-dependency also affects the mechanical behavior of the adhesive layer as its size scales down: the adhesive stiffening can be highlighted through the interfacial jump values which significantly diminishes as the size ratio increases (Figure 4b).

Figure 5 depicts the trends of the interfacial normal stress $t_{33}(x_1) = \frac{1}{h} f(l)(\lambda + 2\mu)[w](x_1)$ and shear stress $t_{13}(x_1) = -\frac{h_b}{h} f(l)\mu\langle w' \rangle(x_1)$ along the axis coordinate in comparison with their elastic counterparts. The diagrams highlight a size-dependent behavior as the size ratio h/ℓ_a decreases, for both normal and shear interface stresses. Especially, the normal stress tends to rapidly increase at the extremities of the layered beam, due to the presence of high strain gradients. As the internal length scale approaches the adhesive thickness, the interfacial stress values of the strain gradient model converge toward the classical elastic solution. Finally, Figure 6 shows the variation of the axial stress $\sigma_{11}^{\pm}(x_1, x_3) = -E\left(x_3 \pm \frac{h_b}{2}\right) w''_{\pm}(x_1)$ across the thickness of the laminated beams, that is, along x_3, for $x_1 = L/2$. As seen in the plot, a decrease of the size ratio h/ℓ_a results in a reduction in the axial stress throughout the laminated structure. The above observation emphasizes the importance of strain gradient elasticity for the analysis of laminated structures and their size-

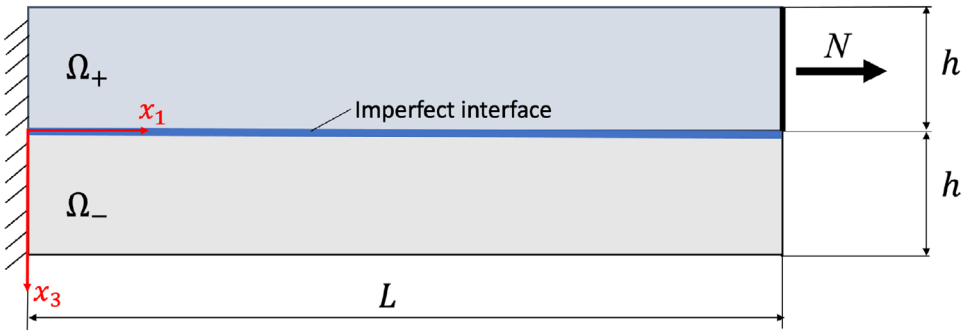

FIGURE 7 Laminated beam under a mode2-type axial loading.

dependent behavior. The present model, which is built using the Euler–Bernoulli kinematical hypothesis for the top and bottom beams, presents some limitations since it is valid in the case of thin laminae. Indeed, the distribution of stresses is piece-wise linear through the thickness and the model do not take into account the possible independent rotations of the transversal fibers, and thus, shear strains. Considering thicker adherents, higher order kinematics can be used such as Timoshenko, higher-order shear deformable theory or unified formulations, see for example, Caliri et al. [2] for a detailed overview. These higher-order theories are used to properly approximate the nonlinear distribution of transverse shear strains along the beam thickness and interlaminar stresses.

4.2 | A mode 2-type axial problem for a strain gradient elastic laminated beam

Let us consider two strain gradient elastic beams, bonded together by a strain gradient adhesive, constituting a mode 2-type shear sliding configuration, as depicted in Figure 7. In the sequel, we neglect any kind of bending coupling. We consider the same geometry features of the previous example, that is, $h^+ = h^- := h_b$ and $E_+ = E_- := E$.

The governing Equation (13) can be adapted to the present case of study, as follows:

$$\begin{cases} EA(\ell_b^2 \bar{u}_+^{(4)} - \bar{u}_+'') + \frac{f(l)}{h}\mu[\bar{u}] = 0 & x_1 \in (0, L), \\ EA(\ell_b^2 \bar{u}_-^{(4)} - \bar{u}_-'') - \frac{f(l)}{h}\mu[\bar{u}] = 0 & x_1 \in (0, L), \\ \bar{u}_\pm = 0 & x_1 = 0, \\ \bar{u}_\pm'' = 0 & x_1 = 0, \\ EA(\bar{u}_+' - \ell_b^2 \bar{u}_+''') = N & x_1 = L, \\ EA(\bar{u}_-' - \ell_b^2 \bar{u}_-''') = 0 & x_1 = L, \\ \bar{u}_\pm' = \epsilon_\pm & x_1 = L, \end{cases} \tag{16}$$

where $\epsilon_\pm$ represents assigned longitudinal strains on the free end of $\Omega_\pm$. The linear system (16) can be solved by employing the same solution strategy adopted in Section 4.1, working on the jump and mean values of the axial displacement. Thus, the general integrals take the following closed-form expressions:

$$\bar{u}_\pm(x_1) = b_1 \ell_b^2 e^{\frac{x_1}{\ell_b}} + b_1 \ell_b^2 e^{-\frac{x_1}{\ell_b}} + b_3 + b_4 x_1 \pm \frac{1}{2}\left(b_5 e^{\theta_1 \frac{x_1}{\ell_b}} + b_6 e^{-\theta_1 \frac{x_1}{\ell_b}} + b_7 e^{\theta_2 \frac{x_1}{\ell_b}} + b_8 e^{-\theta_2 \frac{x_1}{\ell_b}} \right),$$

where $\theta_{1,2} := \sqrt{\frac{1 \mp \rho}{2}}$, with $\rho := \sqrt{1 - \frac{8 f(l) l_b^2 \mu}{EAh}}$, and b_K, $K = 1, \dots, 6$, are the integration constants to be found by applying the boundary conditions.

Let us consider the following numerical example. The adherents $\Omega_\pm$ and the adhesive present the same material parameters indicated in Table 1. We consider the same geometric characteristics of the example in Section 4.1, namely L =10 mm, h_b =1 mm, l_b =0.1 mm, and h =0.1 mm. The axial load is N =10 N. The internal length of the adhesive ℓ_a varies in the same set of size ratios defined in Table 2.

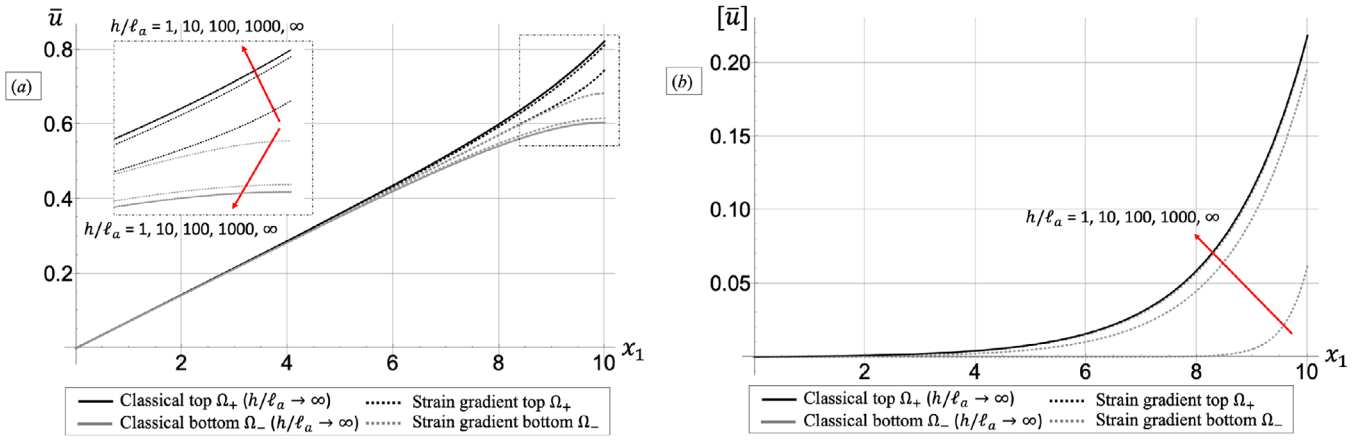

FIGURE 8 Axial displacement $\bar{u}$ (a) and interfacial displacement jump $[\bar{u}]$ (b) versus x_1.

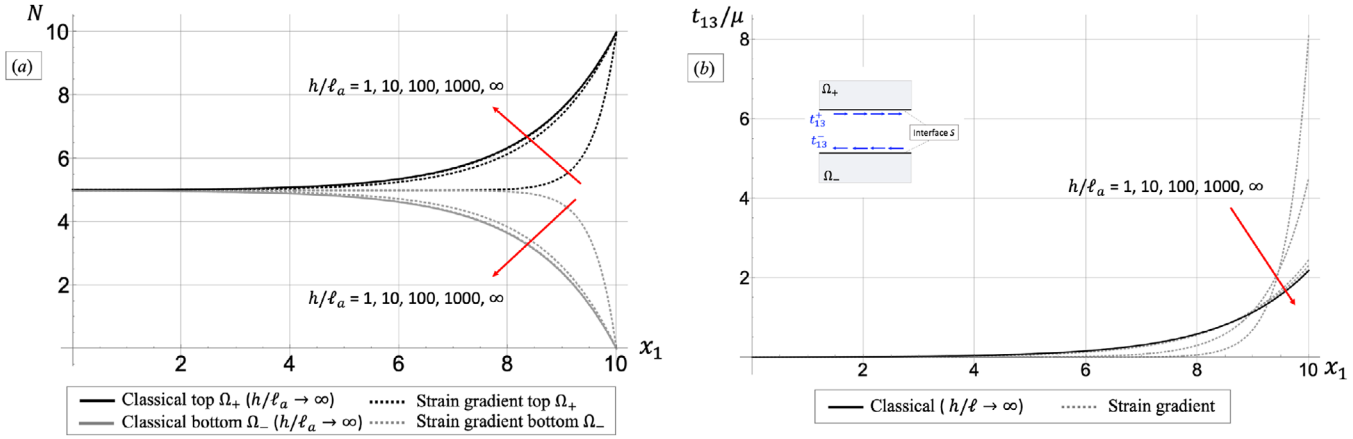

FIGURE 9 Normal force (a) and normalized interfacial shear stress (b) versus x_1.

In Figure 8 the comparison between the classical elastic solution (black and gray continuous lines) and the strain gradient elastic solution (black and gray dotted lines) for different values of the size ratio h/ℓ_a in terms of the axial displacement for the top and bottom beams, and interfacial jump is depicted. As already highlighted in the previous section, the size ratio between the thickness and the internal length of the adhesive significantly influences the mechanical response of the laminated beam. As $h/\ell_a \to \infty$, that is, $\ell_a = 0$, the strain gradient solution converges towards the elastic one. Even for the axial case, the structure presents a size effect phenomenon, involving a global stiffening of the laminated beam when h/ℓ_a tends to 1, see Figure 8a. The stiffening effect can also be seen from the jump of the axial displacement (Figure 8b), which decreases for small values of the size ratio and is concentrated in a more narrow region close to the free end. Thus, a decrease of h/ℓ_a implies a stiffer adhesive and a globally less deformable beam.

Figure 9 depicts the trends of the normal force N and the interfacial shear stress $t_{13}(x_1) = \frac{1}{h} f(l)\mu[\bar{u}](x_1)$ along the x_1-coordinate in comparison with their elastic counterparts. The diagrams highlight a size-dependent behavior as the size ratio h/ℓ_a decreases, for both normal force and interfacial shear interface stress. Concerning the shear stresses at the interface, it is possible to notice a stress concentration close to the free end of the beam due to the high strain gradients.

5 | CONCLUSIONS

This paper investigates the mechanical behavior of a strain gradient laminated beam, made of two strain gradient elastic Euler–Bernoulli beams bonded together by a weak strain gradient elastic adhesive. The presence of the soft intermediate layer is taken into account by means of a novel form of imperfect interface spring-type conditions, obtained in Serpilli et al. [55] through a rigorous asymptotic analysis, and modeling the mechanical behavior of soft strain gradient elastic adhesive, inserted between two adherents. The adopted contact law, apparently equivalent to the classical elastic one, contains an

internal length function $f(l)$, responsible for size effect phenomena. This work represents a natural continuation and application of the theoretical modeling provided in ref. [55]. The variational formulation of the imperfect interface model has been derived and used to obtain the governing equations of the problem (13), divided into bending and extensional equations. It is interesting to notice that the differential system is fully coupled: the terms Λ_1 and Λ_2, associated with the imperfect contact model and representing the interface shear and peeling stresses, respectively, induce the coupling not only of the upper and lower beams equations but also of the extensional and bending behaviors. This work enhances the models developed by other researchers, which do not take into account imperfect contact conditions at the interface among each lamina [35, 36] or the strain gradient nature of the adherents [37]. Two benchmark problems have been presented: the first one deals with the bending of a simply supported strain gradient elastic laminated beam under distributed constant loading; the second one is a mode 2-type axial problem for a strain gradient elastic laminated beam. For both problems, closed-form solutions are available. The numerical results showed the following interesting common features:

1. The adhesive internal length parameter influences the trend of the general solution and its effect becomes more prominent when $h/\ell_a = 1$, highlighting a stiffening phenomenon, mainly due to the high strain gradients. Not only does the strain gradient laminated beam appear to be globally more rigid with respect to the elastic one, but also the adhesive becomes more and more stiff.
2. As $h/\ell_a \to \infty$, that is, $\ell_a = 0$, the solution converges toward the elastic case.
3. The interfacial stresses show a size-dependent behavior as the size ratio $h/\ell_a \to$ decreases, highlighting stress concentrations close to the extremities of the beam due to the high strain gradients.

The above observation emphasizes the importance of strain gradient elasticity for the analysis of laminated structures and their size-dependent behavior. The proposed methodology exhibited efficacy and adaptability, suitable for diverse applications involving laminated beams at the micro-scale. The numerical example provides a preliminary evaluation of the imperfect contact law. For comprehensive computational validation, the interface variation problem (5) should be implemented into a general FE code to perform detailed three-dimensional numerical simulations, thereby offering extensive validation.

ACKNOWLEDGMENTS

Open access publishing facilitated by Universita Politecnica delle Marche, as part of the Wiley - CRUI-CARE agreement.

CONFLICT OF INTEREST STATEMENT

The authors declare no conflicts of interest.

ORCID

Michele Serpilli https://orcid.org/0000-0002-4652-9386
Reinaldo Rodríguez Ramos https://orcid.org/0000-0002-3093-6948
Frédéric Lebon https://orcid.org/0000-0001-8271-5314

REFERENCES

[1] Caliri, M.L.J., Volnei, T., Ferreira, A.J.M.: New generalized unified solution method for thin laminated plates. AIAA J. 54(8), 2555–2559 (2016)
[2] Caliri, M.L.J., Ferreira, A.J.M., Volnei, T.: A review on plate and shell theories for laminated and sandwich structures highlighting the finite element method. Comp. Struct. 156, 63–77 (2016)
[3] Caliri, M.L.J., Ferreira, A.J.M., Volnei, T.: A new finite element for thick laminates and sandwich structures using a generalized and unified plate theory. Int. J. Num. Meth. Eng. 109, 290–304 (2017)
[4] Han, L., Wang, X.D., Sun, Y.: The effect of bonding layer properties on the dynamic behaviour of surface-bonded piezoelectric sensors. Int. J. Solids Struct. 45(21), 5599–5612 (2008)
[5] Jin, C., Wang, X.: Analytical modelling of the electromechanical behaviour of surface-bonded piezoelectric actuators including the adhesive layer. Eng. Fract. Mech. 79(13), 2547–2562 (2011)
[6] Luo, Q.T., Tong, L.Y.: Exact static solutions to piezoelectric smart beams including peel stresses. II. numerical results, comparison and discussion. Int. J. Solids Struct. 39(18), 4697–4722 (2002)
[7] Liu, P., Liu, J., Zhu, X., Wu, C., Liu, Y.: A highly adhesive flexible strain sensor based on ultra-violet adhesive filled by graphene and carbon black for wearable monitoring. Compos. Sci. Technol. 182, 107771 (2019)

[8] Bleiker, S.J., Visser Taklo, M.M., Lietaer, N., Vogl, A., Bakke, T., Niklaus, F.: Cost-efficient wafer-level capping for MEMS and imaging sensors by adhesive wafer bonding. Micromachines 7(10), 192 (2016)

[9] Najar, F., Choura, S., El-Borgi, S., Abdel-Rahman, E.M., Nayfeh, A.H.: Modeling and design of variable-geometry electrostatic microactuators. J. Micromech. Microeng. 15(3), 419 (2004)

[10] Lam, D.C.C., Choura, S., El-Borgi, S., Abdel-Rahman, E.M., Nayfeh, A.H.: Experiments and theory in strain gradient elasticity. J. Mech. Phys. Solids 51(8), 1477–1508 (2003)

[11] Fleck, N.A., Muller, G.M., Ashby, M.F., Hutchinson, J.W.: Strain gradient plasticity: theory and experiment. Acta Metall. Mater. 42(2), 475–487 (1994)

[12] Ji, G., Ouyang, Z., Li, G., Ibekwe, S., Pang, S.S.: Effects of adhesive thickness on global and local mode-i interfacial fracture of bonded joints. Int. J. Solids Struct. 47(18–19), 2445–2458 (2010)

[13] Yang, S., Xu, W., Liang, L., Wang, T., Wei, Y.: An experimental study on the dependence of the strength of adhesively bonded joints with thickness and mechanical properties of the adhesives. J. Adhes. Sci. Technol. 28(11), 1055–1071 (2014)

[14] Campilho, R., Moura, D.C., Banea, M.D., Silva, dL.F.M.: Adhesive thickness effects of a ductile adhesive by optical measurement techniques. Int. J. Adhes. 57, 125–132 (2015)

[15] Mindlin, R.D., Tiersten, H.F.: Micro-structure in linear elasticity. Arch. Rational Mech. Anal. 16, 51–78 (1964)

[16] Mindlin, R.D., Eshel, N.N.: On first strain-gradient theories in linear elasticity. Int. J. Solids Struct. 4, 109–124 (1968)

[17] Aifantis, E.C.: On the role of gradients in the localization of deformation and fracture. Int. J. Eng. Sci. 30, 1279–1299 (1992)

[18] Ru, C.Q., Aifantis, E.C.: A simple approach to solve boundary value problems in gradient elasticity. Acta Mech. 101, 59–68 (1993)

[19] Altan, B.S., Aifantis, E.C.: On some aspects in the special theory of gradient elasticity. J. Mech. Behav. Mater. 8(3), 231–282 (1997)

[20] Askes, H., Suiker, A.S.J., Sluys, L.J.: A classification of higher-order strain-gradient models linear analysis. Arch. Appl. Mech. 72, 171–188 (2002)

[21] Askes, H., Metrikine, A.V.: Higher-order continua derived from discrete media: continualization aspects and boundary conditions. Int. J. Solids Struct. 42, 187–202 (2005)

[22] Askes, H., Aifantis, E.C.: Gradient elasticity theories in statics and dynamics - a unification of approaches. Int. J. Fract. 139, 297–304 (2006)

[23] Polizzotto, C.: Gradient elasticity and nonstandard boundary conditions. Int. J. Solids Struct. 40, 7399–7423 (2005)

[24] Polizzotto, C.: A gradient elasticity theory for second-grade materials and higher order inertia. Int. J. Solids Struct. 49, 2121–2137 (2012)

[25] Polizzotto, C.: A unifying variational framework for stress gradient and strain gradient elasticity theories. Int. J. Solids Struct. 49(15), 430–440 (2015)

[26] Polizzotto, C.: A note on the higher order strain and stress tensors within deformation gradient elasticity theories: Physical interpretations and comparisons. Int. J. Solids Struct. 90(15), 116–121 (2016)

[27] Polizzotto, C.: A second strain gradient elasticity theory with second velocity gradient inertia - part I: Constitutive equations and quasi-static behavior. Int. J. Solids Struct. 50, 3749–3765 (2013)

[28] Askes, H., Aifantis, E.C.: Gradient elasticity in statics and dynamics: An overview of formulations, length scale identification procedures, finite element implementations and new results. Int. J. Solids Struct. 48, 1962–1990 (2011)

[29] Lazopoulos, K.A., Lazopoulos, A.K.: Bending and buckling of thin strain gradient elastic beams. Eur. J. Mech. A. Solids 29, 837–843 (2010)

[30] Xu, L., Shuling, H., Shengping, S.: A new Bernoulli–Euler beam model based on a simplified strain gradient elasticity theory and its applications. Compos. Struct. 111, 317–323 (2014)

[31] Niiranen, J., Balobanov, V., Kiendl, J., Hosseini, S.B.: Variational formulations, model comparisons and numerical methods for Euler–Bernoulli micro- and nano-beam models. Math. Mech. Solids 24(1), 312–335 (2019)

[32] Binglei, W., Junfeng, Z., Shenjie, Z.: A micro scale timoshenko beam model based on strain gradient elasticity theory. Eur. J. Mech. A. Solids 29, 591–599 (2010)

[33] Tajalli, S.A., Rahaeifard, M., Kahrobaiyan, M.H., Movahhedy, M.R., Akbari, J., Ahmadian, M.T.: Mechanical behavior analysis of size-dependent micro-scaled functionally graded Timoshenko beams by strain gradient elasticity theory. Compos. Struct. 102, 72–80 (2013)

[34] Li, A., Zhou, S., Zhou, S., Wang, B.: A size-dependent bilayered microbeam model based on strain gradient elasticity theory. Compos. Struct. 108, 259–266 (2014)

[35] Sidhardh, S., Ray, M.C.: Exact solution for size-dependent elastic response in laminated beams considering generalized first strain gradient elasticity. Compos. Struct. 204, 31–42 (2018)

[36] Guangyang, F., Shenjie, Z., Lu, Q.: The size-dependent static bending of a partially covered laminated microbeam. Int. J. Mech. Sci. 152, 411–419 (2019)

[37] Long, H., Ma, H., Wei, Y., Liua, Y.: A size-dependent model for predicting the mechanical behaviors of adhesively bonded layered structures based on strain gradient elasticity. Int. J. Mech. Sci. 198, 106348 (2021)

[38] Geymonat, G., Krasucki, F., Lenci, S.: Mathematical analysis of a bonded joint with a soft thin adhesive. Math. Mech. Solids 16, 201–225 (1999)

[39] Lebon, F., Rizzoni, R.: Asymptotic analysis of a thin interface: The case involving similar rigidity. Int. J. Eng. Sci. 48, 473–486 (2010)

[40] Lebon, F., Rizzoni, R.: Asymptotic behavior of a hard thin linear interphase: An energy approach. Int. J. Solids Struct. 48, 441–449 (2011)

[41] Rizzoni, R., Dumont, S., Lebon, F., Sacco, E.: Higher order model for soft and hard elastic interfaces. Int. J. Solids Struct. 51, 4137–4148 (2014)

[42] Serpilli, M., Rizzoni, R., Lebon, F., Dumont, S.: An asymptotic derivation of a general imperfect interface law for linear multiphysics composites. Int. J. Solids Struct. 180–181, 97–107 (2019)

[43] Dumont, S., Serpilli, M., Rizzoni, R., Lebon, F.: Numerical validation of multiphysic imperfect interfaces models. Front. Mater. 158, 1–13 (2020)
[44] Serpilli, M., Dumont, S., Rizzoni, R., Lebon, F.: Interface models in coupled thermoelasticity. Technologies 9(1), 17 (2021)
[45] Serpilli, M.: Mathematical modeling of weak and strong piezoelectric interfaces. J. Elast. 121(2), 235–254 (2015)
[46] Serpilli, M., Rizzoni, R., Dumont, S., Lebon, F.: Higher order interface conditions for piezoelectric spherical hollow composites: Asymptotic approach and transfer matrix homogenization method. Compos. Struct 279, 114760 (2022)
[47] Serpilli, M.: Asymptotic interface models in magneto-electro-thermo-elastic composites. Meccanica 52(6), 1407–1424 (2017)
[48] Serpilli, M.: Classical and higher order interface conditions in poroelasticity. Ann. Solid Struct. Mech. 11, 1–10 (2019)
[49] Serpilli, M., Lenci, S.: Asymptotic modelling of the linear dynamics of laminated beams. Int. J. Solids Struct. 49(9), 1147–1157 (2012)
[50] Serpilli, M., Lenci, S.: An overview of different asymptotic models for anisotropic three-layer plates with soft adhesive. Int. J. Solids Struct. 81, 130–140 (2016)
[51] Rizzoni, R., Dumont, S., Lebon, F., Sacco, E.: Higher order adhesive effects in composite beams. Eur. J. Mech. A. Solids 85, 104108 (2021)
[52] Furtsev, A., Rudoy, E.: Variational approach to modeling soft and stiff interfaces in the kirchhoff-love theory of plates. Int. J. Solids Struct. 202, 562–574 (2020)
[53] Serpilli, M.: On modeling interfaces in linear micropolar composites. Math. Mech. Solids 23(4), 667–685 (2018)
[54] Serpilli, M., Rizzoni, R., Rodriguez-Ramos, R., Lebon, F., Dumont, S.: A novel form of imperfect contact laws in flexoelectricity. Compos. Struct. 300, 116059 (2022)
[55] Serpilli, M., Rizzoni, R., Lebon, F., Raffa, M.L., Rodriguez-Ramos, R.: A size-dependent imperfect interface model for adhesively bonded joints considering strain gradient elasticity. Int. J. Solids Struct. 291, 112720 (2024)
[56] Ciarlet, P.G.: Mathematical Elasticity, Vol. II: Theory of Plates. North-Holland, Amsterdam (1997)

How to cite this article: Serpilli, M., Rizzoni, R., Ramos, R.R., Lebon, F.: A size-dependent model of strain gradient elastic laminated micro-beams with a weak adhesive layer. Z Angew Math Mech. e202400609 (2024). https://doi.org/10.1002/zamm.202400609

APPENDIX: ROOTS OF THE CHARACTERISTIC JUMP AND MEAN VALUE EQUATIONS

The characteristic equation associated with the homogeneous jump differential equation in system (15) is:

$$\eta^6 - \alpha_1\eta^4 - \alpha_3 = 0,$$

where $\alpha_1 := \frac{I+\ell_b^2 A}{\ell_b^2 I}$ and $\alpha_3 := \frac{2f(l)(\lambda+2\mu)}{hEI\ell_b^2}$. By following a similar approach developed in Long et al. [37], and considering $\zeta = \eta^2 - \frac{\alpha_1}{3}$, one has:

$$\zeta^3 + 3\beta_1\zeta^2 - 2\beta_2 = 0,$$

with $\beta_1 := -\frac{\alpha_1^2}{9}$ and $\beta_2 := \frac{2\alpha_1^3+27\alpha_3}{54}$. The roots of the above equations are:

$$\zeta_1 = \beta_3 \quad \text{and} \quad \zeta_{2,3} = \frac{\beta_3}{2} \pm \frac{\sqrt{3}}{2}\beta_4 i,$$

with $i = \sqrt{-1}$, $\beta_{3,4} := \sqrt[3]{\beta_2 + \sqrt{\Delta}} \pm \sqrt[3]{\beta_2 - \sqrt{\Delta}}$, where $\Delta := \beta_1^3 + \beta_2 > 0$ is positive for typical materials. Now, we can go back to the initial solutions:

$$\eta_{1,2} = \pm\sqrt{\frac{\alpha_1}{3} + \beta_3},\ \eta_{3,4} = \gamma_1 \pm \gamma_2 i,\ \eta_{5,6} = -\gamma_1 \pm \gamma_2 i,$$

with $\gamma_{1,2} := \sqrt{\frac{1}{2}\left(\sqrt{\left(\frac{\alpha_1}{3} - \frac{\beta_3}{2}\right)^2 + \frac{3\beta_4^2}{4}} \pm \left(\frac{\alpha_1}{3} - \frac{\beta_3}{2}\right)\right)}$. Thus, the general integral is straight-forward.

The characteristic equation associated with the homogeneous mean value differential equation in system (15) is:

$$\tilde{\eta}^6 - \alpha_1 \tilde{\eta}^4 + \alpha_4 \tilde{\eta}^2 = 0,$$

where $\alpha_4 := \frac{h_b^2 f(l)\mu}{2h\ell_b^2 EI}$, whose roots take the following expression, as customary:

$$\tilde{\eta}_{1,2} = \pm\delta_1,\ \tilde{\eta}_{3,4} = \pm\delta_2,\ \tilde{\eta}_{5,6} = 0,$$

where $\delta_{1,2} = \sqrt{\frac{\alpha_1 \mp \sqrt{\alpha_1^2 + 4\alpha_4}}{2}}$. For typical materials, coefficients $\delta_{1,2}$ are real numbers. Then, the general solution of the differential equation can be easily computed.